

Desalination by directional freezing: an experimental investigation

Mona M. Naim^a, Mahmoud M. Elewa^{b,*}, Abeer A. Moneer^c, Ahmed A. El-Shafei^d

^aFaculty of Engineering, Alexandria University, Alexandria, Egypt, email: monanaim66@gmail.com

^bArab Academy for Science, Technology and Maritime Transport, Alexandria, Egypt, email: mahmoud.elewa@gmail.com

^cNational Institute of Oceanography and Fisheries, Alexandria, Egypt, email: yrwah@yahoo.com

^dFaculty of Agriculture, Alexandria University, Alexandria, Egypt, email: ahmed.elshafi@alexu.edu.eg

Received 30 October 2016; Accepted 1 February 2017

ABSTRACT

Desalination of saline waters by freezing is one of the oldest methods for desalination, which relies on the principle that the ice crystal structure cannot accommodate salts during its formation, and salts are rejected during phase transformation. Despite its numerous merits as compared to thermal desalination processes, such as low energy requirements, minimum corrosion potential and no scale formation on surfaces, and its suitability for remote areas, small societies, and cold regions, yet it has been neglected during the last few decades. In the present work, an investigation was conducted to determine the effect of directional freezing on the salinity of the produced ice. Containers of different configurations and sizes, which were filled with saline water of different initial concentrations, were subjected to gradual freezing, then sliced into several equal sections from top to bottom, and the ice allowed to melt in separate containers, while other configurations were sliced into circular annular sections of different radii, then all the samples were analyzed for NaCl. Variables studied for their effect on the salinity, included container configuration, initial saline concentration (C_i) (5, 15, 25 and 35 g/L), and vertical/radial distances. It was found that concentration increased from periphery to center and from top to bottom. The freezing and solubility curves of NaCl-water system were calculated using the perturbed-chain statistical associating fluid theory (PC-SAFT) with the corresponding melting temperatures and enthalpies of fusion of the pure substances using the binary parameter (k_{ij}) of -0.1793 for NaCl-water system.

Keywords: Desalination; Freezing; Directional freezing; PC-SAFT model

1. Introduction

Water means life. Without water, our earth would be a dead planet. However, due to the rapid and continuous increase in population, particularly in the last few decades, a strong lack of potable water is posing itself as a worldwide problem, which has to be solved one way or other. Accordingly, to solve this problem, the only possible solution was to desalinate ocean- and sea- waters, which constitute 97% of the total water present on the planet [1]. Numerous firmly entrenched techniques have posed themselves

lately, such as multistage flash (MSF), multi-effect distillation (MED), vapor compression distillation (VCD), reverse osmosis (RO), and electrodialysis reversal (EDR) [1]. However, the search for other novel or minor techniques, which are more energy-saving is always carried out. On the other hand, there are other less common techniques which are developing nowadays such as desalination by membrane distillation (MD) [2–4], humidification-dehumidification of air (H-D) [5–7], ion exchange (IE) [8,9], solar distillation [10–12], pervaporation (PV) [13–16], liquid membranes (LMs) [17–19], electrosorptive desalination (also called capacitive

*Corresponding author.

Presented at the EDS conference on Desalination for the Environment: Clean Water and Energy, Rome, Italy, 22–26 May 2016.

deionization) [20–24] and freeze desalination (FD) [25–30]. Moreover, new trends using hybrid systems such as FD-MD have been developing recently [31].

As regards applying freezing to desalination, it is a well-known process, which relies on the principle that the structure of a single ice crystal does not accommodate salts, since during freezing of a salt solution salts are rejected by the growing ice crystal. The ice crystals can then be separated from the concentrated brine, then melted to yield pure water. However, despite that several merits are claimed for freezing over other methods, yet it has not reached technical maturity although the latent heat of fusion of ice is only 335 kJ/kg while that of vaporization is 2500 kJ/kg [32], which, however, does not mean that freezing is thermodynamically a more stable process, but merely means that thermodynamic losses in heat exchange are minimized [32].

No full-scale commercial freeze desalinator has yet been built, despite this advantage only freeze concentrators have successfully applied the principle. The reason is that no significant savings in total costs have been gained over other more established methods, due to its high capital and operating costs. The concept of freeze desalination (FD) dates back to the 1950's, and most of the literature of the subject dates back to the 50's, 60's, and 70's [33–36]. When freezing brine, the ice crystal will reject the solute and will continuously freeze out "the water part", as a result the concentration of the solution in the fluid will increase steadily [37]. In a direct freezing process, a refrigerant is mixed directly with the brine, while, in an indirect process, the refrigerant is separated from the brine by a heat transfer surface [38]. Hybrid ICE™ is an environmentally friendly and economically feasible technology for most freezing processes. In principle, a Hybrid ICE™ generator is a scraped surface, double-walled heat exchanger, in which in the outer annular space, a primary refrigerant is circulated. As a result, the ice crystals form on the cooled inside surface of the inner tube and are continuously being removed from the surface by rotating glide-scrapers mounted on a rotor [38]. The technique has proven to be cost-effective, less polluting with by-products, simple, and has the ability to generate cold energy from the process. In addition, the results have shown that the energy consumption is lower than evaporation processes. An example of a direct FD process is the Zarchin process, in which water itself is used as a refrigerant [38]. However, it must operate under significant vacuum, therefore less work is required per unit fresh water produced.

Shafique, et al. [39] conducted a research on migration of ions by direction freezing of water and redistribution of anions and cations which creates an electrical imbalance in ice grown from electrolyte solutions. Movement of acidic and basic ions in cooling solutions can permanently change the pH of frozen and un-frozen parts of the system, largely. The extent of pH change associated with freezing is determined by solute concentration and the extent of cooling. In their work, redistribution of hydrogen, hydroxyl, carbonate, and bicarbonate ions was studied during directional freezing in batch aqueous systems. Controlled freezing was employed vertically as well as radially in acidic and basic solutions. In each case, the ions substantially migrated along with moving freezing front.

Desalination processes based on freezing have not been exploited because of the operational difficulties in ice–water separation, high cost of equipment and high parasitic power requirement. To this end, Rane and Padiya [29] discussed a patented layer freezing based technology which has competitive initial and operating cost and eliminates operational difficulties of conventional freezing system. It is scalable and is coupled with a heat pump which selectively freezes water from seawater in the evaporator and melts the ice in the subsequent phase when it serves as a condenser. The condenser optimally utilizes the latent heat of melting of ice to partially condense the refrigerant and the excess heat is rejected to ambient. It avoids the need of ice scraper/separation mechanisms. Use of vented-double-wall tube-tube heat exchanger (TT-HE) enables refrigerant and seawater/potable water to exchange heat without the use of intermediate fluids, while keeping the inclusion low. TT-HE is a reliable heat exchanger which ensures that refrigerant and seawater/water do not mix. Operating coefficient of performance of the heat pump is in the range of 8–12, which results in specific energy consumption in the range of 9–11 kWh/m³ of water produced. The authors presented a comparison of features with other freezing desalination processes. Non potable RO combined with direct contact freezing (DCF), could reduce the overall energy consumption by about 13% and 17% when compared with separate RO and DCF plants respectively, along with reduction in brine outflow. Here rejected brine from RO is used as feed to freezing system [40].

There are basically two approaches to calculate the freezing curve of the solid complex: one method is to treat the complex formations as chemical reactions described by corresponding equilibrium constants [41,42]. The second approach is to model the complex formation by applying a physical model, e.g. an activity-coefficient model or an equation of state (EOS), which includes strong hydrogen-bonding interactions by introducing additional adjustable parameters [43]. Recently, Tumakaka, et al. [42] applied the perturbed-chain statistical associating fluid theory (PC-SAFT) for EOS to model the solid–liquid equilibria (SLE) of binary and ternary systems (water, alcohols, phenol, bisphenol A) considering complex formation due to hydrogen bonding only in the solid phase. The formation is described as a chemical reaction between the related compounds. A physical model, the PC-SAFT EOS, is combined with the chemical theory, and is used to take into account the non-ideality of the system, i.e. to calculate the activity coefficients in the equilibrium constant. The PC-SAFT EOS has been successfully applied earlier to pure components and mixed fluids including non-polar, polar and associating substances as well as to polymers and copolymers [44–48]. The molecular model underlying the PC-SAFT EOS takes into account the effects of hard-chain formation, dispersive attraction and association interactions and is proved to be physically based and robust for representing complex fluids exhibiting specific interactions (hydrogen bonding) between molecules [42].

In the present work an investigation of the direction of motion of salt ions relative to water, during the freezing of saline water, seawater and CuSO₄ at different rates, different initial concentrations, and containers of different shapes and sizes, was carried out. The PC-SAFT EOS was applied to model the SLE of freezing systems.

2. Materials and methods

Four containers of different sizes and shapes as shown in Fig. 1, were filled with seawater (Table 1) and saline water of different concentrations (5, 15, 25 and 35 g/L) of NaCl and $\text{CuSO}_4 \cdot 5\text{H}_2\text{O}$, and made to stand upright in a refrigerator ice-box, and left to freeze at -5 , -10 and -15°C for 24 h. Each long container containing its ice, was sliced into equal sections from top to bottom, and the ice allowed to melt in separate containers. The frozen ice was sliced as follows: The ice block was loosened from the container by allowing to melt superficially at room temperature, under our supervision. Then, the block was sliced into equal circular horizontal layers using a heated metallic mechanical saw, then rapidly, sliced into segments at the periphery of the circular slices at equal distance from the center all round, followed by placing the segments in one container, to melt for analysis. The operation is repeated for different reduced radii and each product collected in separate container ready for analysis. In addition, analysis of concentrated brine was investigated in the section located at 2 cm from the bottom after melting these sections. Similarly, each wide container with its ice, was sliced into circular annular sections of different radii, and the ice allowed to melt in separate containers. All the samples were then analyzed conductimetrically.

AQ1 Figures were drawn relating C_s (concentration, in g/L) versus height of slice above the bottom of the bottle, and C_s

versus distance of annulus from the center of the trough, for different initial concentrations. The chemical analysis of seawater, which was collected from Mediterranean coast of Alexandria, Egypt, was carried out and presented in Table 1.

2.1. Thermodynamic modeling PC-SAFT equation of state (EOS)

There exist an enormous number of EOS accessible for predicting the phase behavior of chemical systems. In this work, one of the state of the art EOS commonly employed for chemical systems was used, the PC-SAFT EOS, which was presented by Gross and Sadowski [44]. The activity coefficient of a solute compound i in the mixture is evaluated in this work through the PC-SAFT EOS. Utilizing this model, the residual Helmholtz energy (A^{res}) of a system containing the solute compound and solvent(s) is considered as the entirety of different contributions resulting from repulsion (hc: hard chain), van der Waals attraction (disp: dispersion) and hydrogen bonding (assoc : association) as indicated by [42,49]:

$$\frac{A^{\text{res}}}{NkT} = \frac{A^{\text{hc}}}{NkT} + \frac{A^{\text{dis}}}{NkT} + \frac{A^{\text{assoc}}}{NkT} \quad (1)$$

where A is Helmholtz energy [J], N is total number of molecules [–], k is Boltzmann constant [J K^{-1}] and T is tempera-

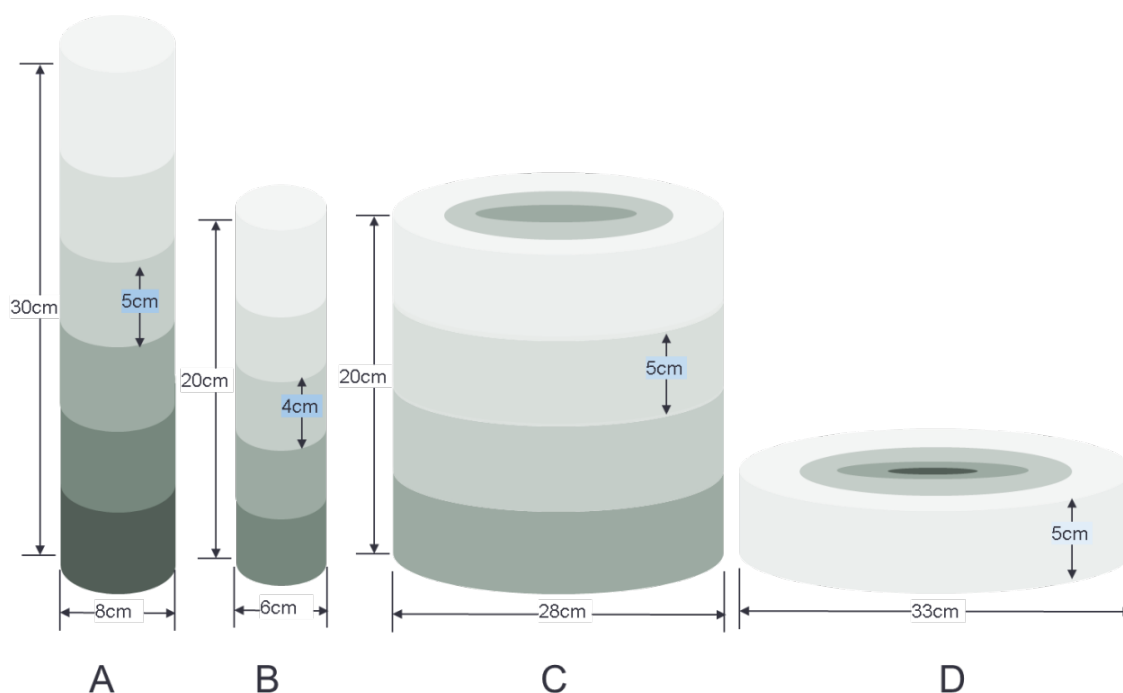


Fig. 1. Sizes and shapes of containers used in experiments.

Table 1
Seawater chemical properties

	TDS (g/L)	Soluble cations (g/L)				Soluble anions (g/L)		
		Ca^{2+}	Mg^{2+}	Na^+	K^+	Br^-	SO_4^{2-}	Cl^-
Average	38.21	0.4004	1.4991	12.335	0.3822	0.0659	3.026	20.94

ture [K]. The different contributions to the Helmholtz energy according to PC-SAFT as well as the model parameters are concisely exhibited below.

2.1.1. Hard-Chain contribution (A^{hc})

The hard-chain reference liquid comprises of spherical fragments, which do not display any attractive collaborations. To describe a hard-chain liquid, two parameters are required, specifically the number of fragments m and their diameter σ . The Helmholtz energy of this reference system is depicted by an expression created by Chapman, et al. [50] which depends on Wertheim's first order thermodynamic perturbation theory [51–53]. The Helmholtz energy of the hard-chain reference term is given as [49]:

$$\frac{A^{hc}}{NkT} = \bar{m} \cdot \frac{A^{hs}}{N_s kT} - \sum_i x_i (m_i - 1) \cdot \ln g_{ii}^{hs}(d_{ii}) \quad (2)$$

where x_i is the mole division of chains of component i , m_i is the number of fragments in a chain and the mean fragment number in the mixture is defined as:

$$\bar{m} = \sum_i x_i m_i \quad (3)$$

The Helmholtz energy for the hard-sphere fragments $A^{hs}/N_s kT$ in Eq. (2) is given on a per-segment basis as [49]:

$$\frac{A^{hs}}{N_s kT} = \frac{1}{\xi_0} \left[\frac{3\xi_1 \xi_2}{(1-\xi_3)} + \frac{\xi_2^3}{\xi_3(1-\xi_3)^2} + \left(\frac{\xi_2^3}{\xi_3^2} - \xi_0 \right) \cdot \ln(1-\xi_3) \right] \quad (4)$$

where N_s is linked to the number of hard-spheres and the radial pair spreading function for the hard-sphere liquid is given by [49]:

$$g_{ij}^{hs}(d_{ij}) = \frac{1}{(1-\xi_3)} + \left(\frac{d_i d_j}{d_i + d_j} \right) \frac{3\xi_2}{(1-\xi_3)^2} + \left(\frac{d_i d_j}{d_i + d_j} \right)^2 \frac{2\xi_2^2}{(1-\xi_3)^3} \quad (5)$$

and ξ_n is defined as:

$$\xi_n = \frac{\pi}{6} \cdot \rho \sum_i x_i m_i d_i^n \quad n = \{0, 1, 2, 3\} \quad (6)$$

where ρ is liquid density. The temperature-dependent fragment diameter is obtained as [49]:

$$d_i = \sigma_i \left(1 - 0.12 \cdot \exp \left(-3 \cdot \frac{\varepsilon_i}{kT} \right) \right) \quad (7)$$

where σ_i is the temperature-independent fragment diameter and ε_i is the depth of the pair-potential. To compute mixture properties (e.g., solute compound i in solvent j), the fragment diameters of the two pure components are joined by means of ordinary Berthelot–Lorentz rules according to:

$$\sigma_{ij} = \frac{1}{2} (\sigma_i + \sigma_j) \quad (8)$$

2.1.2. Dispersion contribution (A^{disp})

The contribution of dispersive attractions (compare to van der Waals connections) to the Helmholtz energy of a system according to PC-SAFT was resulting from the perturbation theory of Barker and Henderson [54,55] applied to the hard-chain reference system.

$$\begin{aligned} \frac{A^{disp}}{NkT} = & -2\pi\rho \cdot I_1(\eta, \bar{m}) \cdot \sum_i \sum_j x_i x_j m_i m_j \left(\frac{\varepsilon_{ij}}{kT} \right) \sigma_{ij}^3 \\ & - \pi\rho \cdot \bar{m} \cdot C_1 I_2(\eta, \bar{m}) \cdot \sum_i \sum_j x_i x_j m_i m_j \left(\frac{\varepsilon_{ij}}{kT} \right)^2 \sigma_{ij}^3 \end{aligned} \quad (9)$$

with

$$\begin{aligned} C_1 = & \left(1 + Z^{hc} + \rho \frac{\partial Z^{hc}}{\partial \rho} \right)^{-1} \\ = & \left(1 + \bar{m} \frac{8\eta - 2\eta^2}{(1-\eta)^4} + (1-\bar{m}) \frac{20\eta - 27\eta^2 + 12\eta^3 - 2\eta^4}{[(1-\eta)(2-\eta)]^2} \right)^{-1} \end{aligned} \quad (10)$$

with η is the packing fraction which equals to ξ_3 in Eq. (6). The power series I_1 and I_2 depend only on the packing fraction and fragment number according to:

$$I_1(\eta, \bar{m}) = \sum_{i=0}^6 a_i(\bar{m}) \cdot \eta^i \quad (11)$$

$$I_2(\eta, \bar{m}) = \sum_{i=0}^6 b_i(\bar{m}) \cdot \eta^i \quad (12)$$

where the coefficients $a_i(\bar{m})$ and $b_i(\bar{m})$ are functions of the segment number:

$$a_i(\bar{m}) = a_{0i} + \frac{\bar{m}-1}{\bar{m}} a_{1i} + \frac{\bar{m}-1}{\bar{m}} \cdot \frac{\bar{m}-2}{\bar{m}} a_{2i} \quad (13)$$

$$b_i(\bar{m}) = b_{0i} + \frac{\bar{m}-1}{\bar{m}} b_{1i} + \frac{\bar{m}-1}{\bar{m}} \cdot \frac{\bar{m}-2}{\bar{m}} b_{2i} \quad (14)$$

The universal model constants in Eqns. (7) and (9) are given in the work of Gross and Sadowski [44].

In addition to the previously mentioned parameters, one extra parameter is required for describing the fragment–fragment interaction of various molecules, which is the dispersion energy parameter ε/k . To calculate the mixture property from pure-component parameters, again conventional Berthelot–Lorentz combining rules are applied:

$$\left(\frac{\varepsilon}{k} \right)_{ij} = \sqrt{\left(\frac{\varepsilon}{k} \right)_i \left(\frac{\varepsilon}{k} \right)_j} \cdot (1 - k_{ij}) \quad (15)$$

Eq. (15) also contains one customizable binary interaction parameter k_{ij} which is used to correct the dispersion energy in the mixture. The value of k_{ij} between solute and solvent is determined from fitting the k_{ij} to binary solubility data. The values of k_{ij} between different solvents were fitted to the binary vapor–liquid equilibria and have already been partly conveyed in the literature [56].

For the description of ternary or multi-component systems it is expected that two-molecule interactions dominate and thus no other than binary parameters are required.

2.1.3. Association contribution (A^{assoc})

The contribution due to short-range association interactions (hydrogen bonding) A^{assoc} is considered by an association model which was suggested by Chapman, et al. [57] based on Wertheim's first-order thermodynamic perturbation theory (TPT1).

$$\frac{A^{assoc}}{NkT} = \sum_i x_i \sum_{A_i=1}^{nsite} \left(\ln X^{A_i} - \frac{X^{A_i}}{2} + \frac{1}{2} \right) \quad (16)$$

Note that the summation runs over all association sites of the molecule i where X^{A_i} is the fraction of the free molecules i that are not bonded at the association site A :

$$X^{A_i} = \left(1 + \rho \cdot \sum_i x_i \sum_{B_j} X^{B_j} \cdot \Delta^{A_i B_j} \right)^{-1} \quad (17)$$

with

$$\Delta^{A_i B_j} = g_{ij}^{hs} \cdot (d_{ij}) \cdot k^{A_i B_j} \cdot \sigma_{ij}^3 \cdot \left(\exp\left(\frac{\epsilon^{A_i B_j}}{kT}\right) - 1 \right) \quad (18)$$

where $g_{ij}^{hs} \cdot (d_{ij})$ is the pair distribution function of hard spheres given in Eq. 5.

Within this theory a molecule is expected to have one or more association sites (electron acceptors or electron donors) which can form hydrogen bonds. The association between two different association sites of the same molecule i is portrayed by two extra parameters: the association strength $\epsilon^{A_i B_i}/k$ and the effective volume of the association interaction $\kappa^{A_i B_i}$. Subsequently, an associating compound is characterized by a total of five pure-component parameters (segment number m , fragment diameter σ , dispersion energy parameter ϵ/k , association strength $\epsilon^{A_i B_i}/k$, and the effective volume of the association interaction $\kappa^{A_i B_i}$).

The quality of cross-association interactions between the association sites of two different compounds (A_i and B_j) can be resolved utilizing basic consolidating principles of the pure-component parameters as proposed by Wolbach and Sandler [58] without introducing any further binary parameters:

$$\frac{\epsilon^{A_i B_j}}{k} = \frac{1}{2} \left(\frac{\epsilon^{A_i B_i}}{k} + \frac{\epsilon^{A_j B_j}}{k} \right) \quad (19)$$

$$\kappa^{A_i B_j} = \sqrt{\kappa^{A_i B_i} \cdot \kappa^{A_j B_j}} \cdot \left(\frac{\sigma_i \cdot \sigma_j}{\frac{1}{2}(\sigma_i + \sigma_j)} \right)^3 \quad (20)$$

Knowing the molecular structure of a molecule, one can pick the terms that must be incorporated in the estimation of the Helmholtz energy. Non polar or weakly-polar components can be satisfactorily depicted utilizing only the hard-chain and dispersion contributions. For associating

compounds, the association contribution also should be considered. For example, for NaCl solution (Fig. 2), two different types of association sites are expected (electron acceptor and electron donor), each of them existing three times per molecule. The two association types were assumed to be of equal strength and range. Therefore, only one value for the association strength ($\epsilon^{A_i B_i}/k$) and one value for the association volume ($\kappa^{A_i B_i}$) parameter need to be determined.

2.2. Solid-liquid phase equilibrium

From the thermodynamic perspective, the solubility can be figured in light of the phase – equilibrium condition for solid and liquid phases, that is, depends on the equality of the chemical potentials of the solute compound (i) in both, solid and liquid phase [49]:

$$\mu_i^L = \mu_i^S \quad (21)$$

In view of that, supposing a pure solid phase and neglecting the difference of solid and liquid heat capacities, the solubility of the solute compound i can be expressed by the following equation [49,59]:

$$x_i^L = \frac{\phi_{oi}^L(T, p)}{\phi_i^L(T, p, x_i^L)} \cdot \exp \left[-\frac{\Delta H_{oi}^{SL}}{RT} \left(1 - \frac{T}{T_{oi}^{SL}} \right) - \frac{(v_{oi}^S - v_{oi}^L) \cdot (p_0 - p)}{RT} \right] \quad (22)$$

where, x_i^L characterizes the solubility of the solute compound i (mole fraction in the liquid phase). ϕ_{oi}^L and ϕ_i^L are the fugacity coefficients of the solute compound i as a pure liquid and in the liquid mixture, respectively. The latter consists of the dissolved solute compound i and the solvent(s). The fugacity coefficients are thermodynamic quantities depending on temperature T and pressure p and are commonly calculated from equations of state. ΔH_{oi}^{SL} and T_{oi}^{SL} are the melting enthalpy and the melting temperature of the pure solute compound i , respectively, whereas R is the gas constant. v_{oi}^S and v_{oi}^L are the molar volumes of the pure solute compound as solid (S) and liquid (L), respectively. p_0 is the standard pressure of 1 bar. Since the molar volume of the solid is not experimentally obtainable and the difference between v_{oi}^S and v_{oi}^L is usually very small, the second term in the exponent can be neglected in the solubility calculations, so that the pressure dependence of the solubility is only taken into account by the fugacity coefficients. In order to calculate the freezing curves of the pure component, Eq. (22) has to be solved iteratively for different temperatures [42].

3. Results and discussion

3.1. Solid–liquid phase diagram

Fig. 3 demonstrates the solid-liquid phase diagram of the NaCl-water system. All the phases are specified in the chart. Above the freezing and solubility curves the mixture is a homogeneous liquid composed of the NaCl solution. Below the freezing and solubility curves, the solid–liquid phase areas are divided into two parts according to the type of the solid formed: pure ice + liquid solution of NaCl, pure solid

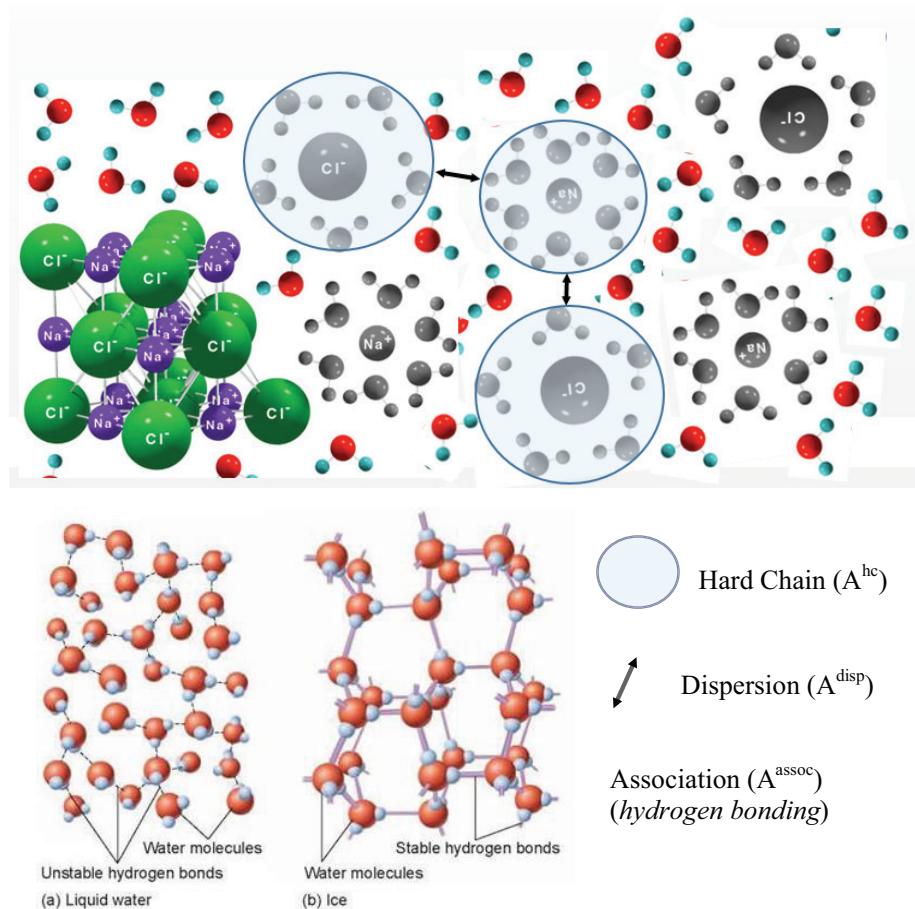


Fig. 2. Molecular model of NaCl solution within the framework of PC-SAFT.

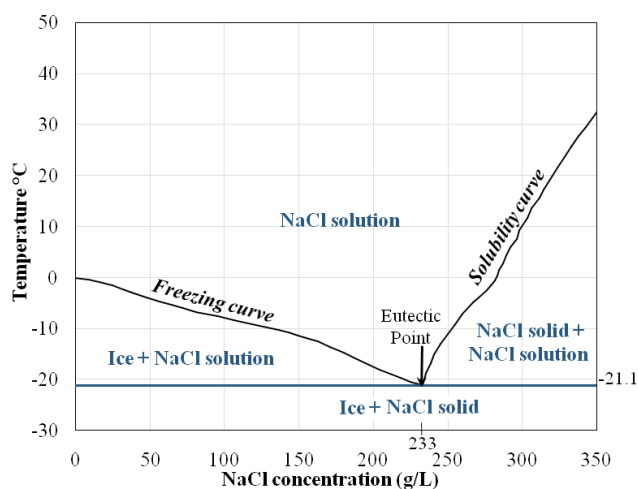


Fig. 3. Solid-liquid phase diagram of the NaCl-water system.

of NaCl+ liquid solution of NaCl. Beneath the solid-liquid phase region, a solid-solid equilibrium with total immiscibility of the respective compounds can be found. Fig. 3 shows the solid-liquid phase diagram of the NaCl-water system which has been considered in literature [60–64]. The

lines characterize the phase boundaries of solid-liquid and solid-solid equilibrium, respectively. The freezing and solubility curves of NaCl-water system were calculated using Eq. (22) with the corresponding melting temperatures and enthalpies of fusion of the pure substances. The binary parameter k_{ij} was fitted to the solubility data and was found to be equal to -0.1793 for NaCl-water system [64].

3.2. Using the phase diagram

The phase diagram was utilized to discover what happens if the salt solution of a specific concentration was cooled. As shown in Fig. 4 (a and b) when the temperature drops sufficiently so that it reaches the boundary between the two areas of the phase diagram, ice crystals start to form, in other words, the solution starts to freeze. As the solution continues to cool, it moves down into the “ice + salt solution” region. Noticeably, the composition of the solution has changed because it contains less water; some of it has frozen to give ice. However, the composition of the system as a whole is still the same, and so the same line was continued down [31,61]. Theoretically, to find out what has happened in the mixture, a horizontal tie line (dashed line) through the freezing temperature was drawn. On the left of the horizontal line, it hits the vertical axis showing 100% water, in this

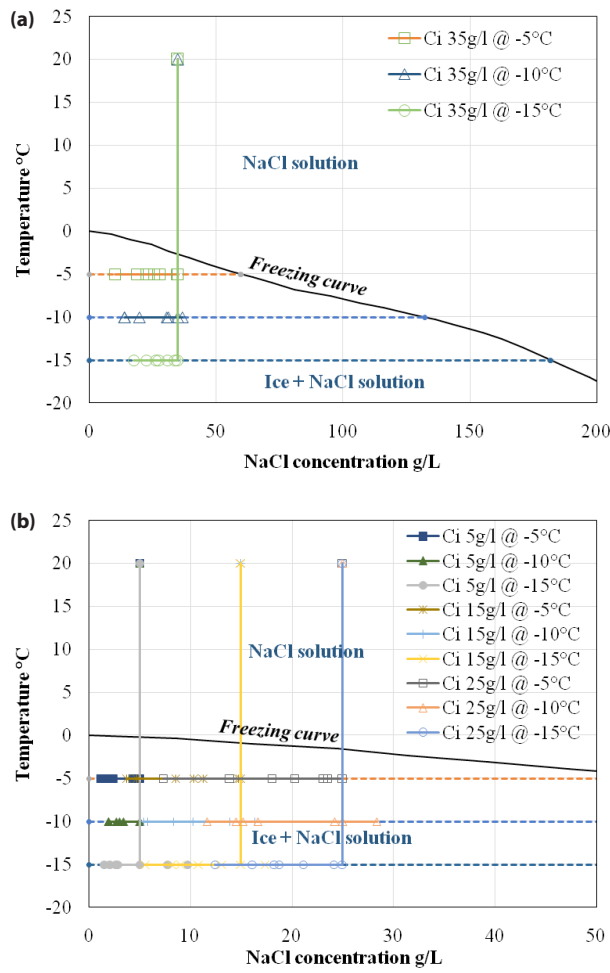


Fig. 4. The frozen slices concentration of container A plotted on solid–liquid phase diagram of the NaCl–water system for cooling temperature of -5 , -10 and -15°C at (a) $C_i = 35\text{ g/L}$, and (b) at C_i of 5 , 15 and 25 g/L .

case, that's the pure ice crystals. On the other end, it hits the freezing curve; this tells the composition of the remaining salt solution. Accordingly, in case of freezing NaCl solution at -5 , -10 and -15°C , the composition of the remaining salt solutions could be 60 , 132 and 182 g/L , respectively (Fig. 4a). However, on actual basis, when four different salt solutions with the concentration of 5 , 15 , 25 and 35 g NaCl/L were cooled from 20°C to -5 , -10 and -15°C in containers of type A (30 cm height and 8 cm diameter as shown in Fig. 1), the concentration profiles overlapped at each cooling temperature (-5 , -10 and -15°C) (Fig. 4), therefore, the concentration profile of each container at each cooling temperature were replotted to demonstrate the variation of concentrations from top to bottom as shown in Figs. 5–7. In the present work the effect of aspect ratio of container containing saline water on the distribution of the salt in the different locations of the container, whether vertically or radially was explored. Furthermore, the effect of rate of cooling was also considered, also the initial salt solution concentration, types of solute (NaCl and copper sulphate penta hydrate were selected) and finally ordinary filtered seawater.

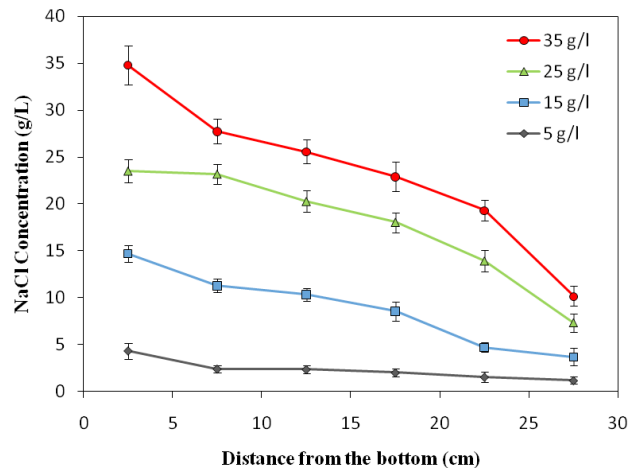


Fig. 5. The concentration profile of the frozen slices of containers A at freezing temperature of -5°C and different initial concentrations of NaCl.

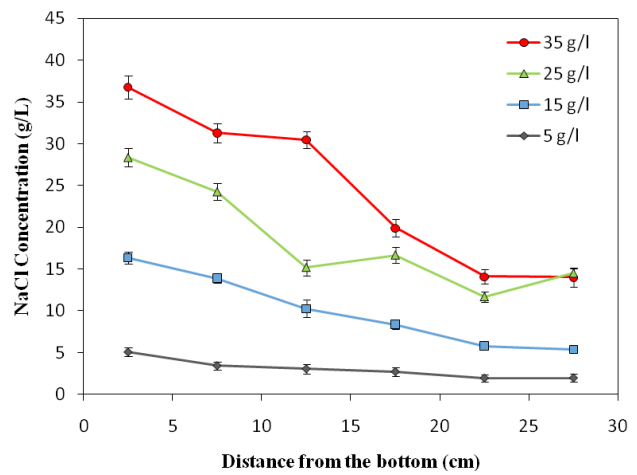


Fig. 6. The concentration profile of the frozen slices of containers A at freezing temperature of -10°C and different initial concentrations of NaCl.

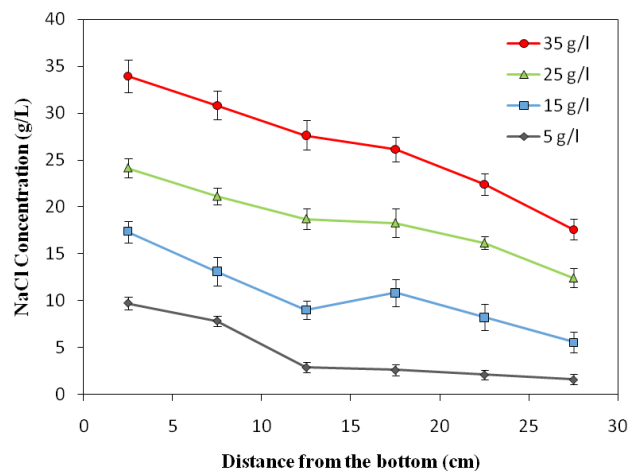


Fig. 7. The concentration profile of the frozen slices of containers A at freezing temperature of -15°C and different initial concentrations of NaCl.

3.3. Effect of rate of freezing

This factor is of great importance, since it is expected that giving more time for the temperature to drop to under freezing temperatures will give the chance to solute to diffuse in the respected direction, thus better desalination is expected. In case of cooling two containers of salt solution and all factors are constant (e.g. size, volume, initial temperature and concentration) and the only difference was that the freezing temperature, in one container was -5°C and the other was -15°C , the salt solution in the -15°C would freeze faster. Therefore, the rate of freezing in this case is dependent on the temperature of the freezer. However, the effect of rate of freezing is depicted in Figs. 5–7. On inspection of Fig. 5, it is observed that at the freezing temperature equal to -5°C , the rate is the slowest, and when C_i equals 35 g/L at the topmost distance (27.5 cm), the concentration is slightly below 10 g/L. While, from Fig. 6, at rate when the freezing temperature is -10°C , the concentration at the same location is slightly below 15 g/L. Furthermore, at rate when the freezing temperature is -15°C as shown in Fig. 7, the concentration at the same aforementioned location was 17.5 g/L, which altogether proves that a slower rate results in better separation. The same observations are realized at the other concentrations

tested (5, 15 and 25 g/L) at the same three rates. On the other hand, the concentration at the bottommost portion (2.5 cm) increases with increasing rate, e.g. when C_i equals 5 g/L at the aforementioned location at the lowest rate the concentration in the thereabout of 4 g/L. Whereas, when the rate increased to the medium rate (-10°C), the concentration is exactly 5 g/L, while, at the highest rate in the present study (-15°C), the concentration became 10 g/L. This observation emphasizes the importance of the rate of freezing due to its control on diffusivity during cooling together with the effect of gravity. Thus, the lower the rate the better separation of salt from the water and therefore desalination is more effective. That also could be attributed to the fact that in the freezing process of a salt solution, there are two types of solids present: ice and salt.

The suspension in an Eutectic Freeze Crystallization, in which the crystallizer can be specified as a bi-disperse suspension. In theory the density difference between the different compounds approves that ice will float to the top and salt will sink to the bottom, which means it is both a clarifying and a thickening process at the same time [65]. The crystallization phenomena are visually described in Fig. 8a. The crystals grow larger when they get more time to grow, they also become larger when multiple particles stick together

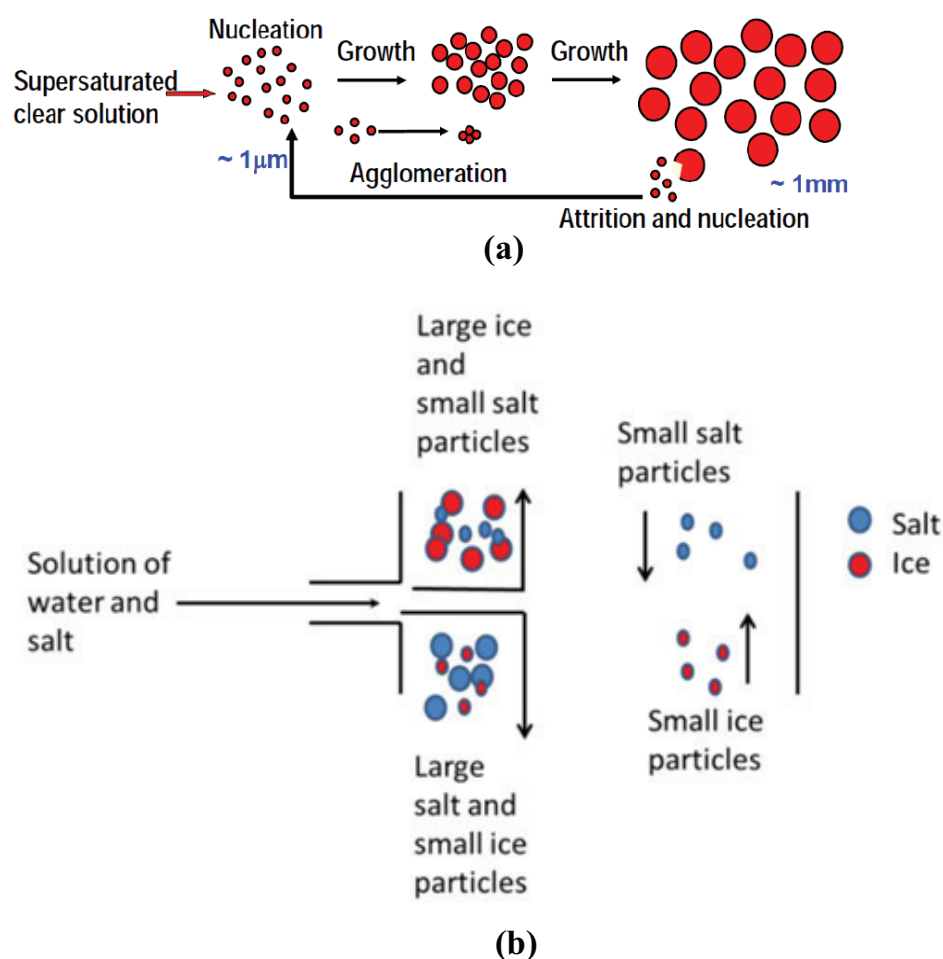


Fig. 8. (a) Crystallization phenomena, (b) Graphical display of the working of a settler column [adapted from van der Tempel [65]].

and form one larger particle. In the case of attrition, large particles become smaller and form new particles. For the settling velocity of single particles this means that growth and agglomeration can increase the settling velocity, while attrition decreases the settling velocity. The particle size of the smallest particles is the restrictive factor to a good separation [65]. This is because the particle size is largely responsible for the settling velocity and small particles have an affinity to move in the 'wrong' direction when the flow velocity is too high. When ice and salt are separated in a column, the upward flow velocity of liquid should not be faster than the downward settling velocity of the smallest salt particles (Fig. 8b). In the same way, the downward flow velocity of liquid should not be faster than the upward velocity of the smallest salt particles. The flow rate of the slurry flow in a settler is usually not governable, but it does influence the flow velocity in the column. The flow velocity in the column is altered to the settling velocity during the design phase by choosing a correct diameter for the column. When the diameter of the column increases with a constant flow rate, then the flow velocity will decrease. This is also why in a water purification plant the sedimentation tanks are so wide in diameter [65]. Conclusively, these phenomena were observed in our investigation so that the brine was concentrated in the bottom most part of the container at about 2 cm from the bottom, in case of lowest freezing rate the brine concentration reached 36, 80, 91 and 149 g/L for C is 5, 15, 25 and 35 g NaCl/L, respectively.

3.4. Effect of aspect ratio

The same experiment using another cylinder (B) of dimensions $L = 20$ cm, and $D = 6$ m was used in testing the four different concentrations C is (5, 15, 25 and 35 g NaCl/L) at rate 1 which was the slowest (at freezing temperature of -5°C). This experiment reveals the effect of aspect ratio L/D on the nature of the progress of freezing operation. Inspecting the figure proves that the smaller the aspect ratio is, the more erratic is the desalination operation by freezing. This is depicted in Fig. 9. A glance at the figure shows that some sort of distortion happens at the concen-

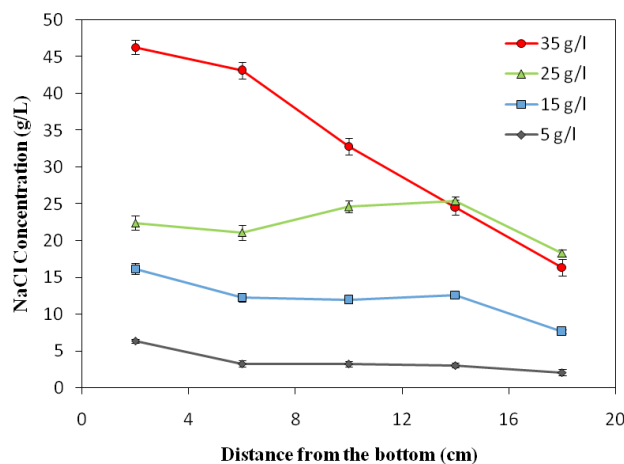


Fig. 9. The concentration profile of the frozen slices of containers B at freezing temperature of -5°C and different initial concentrations of NaCl.

tration of 25 g/L; this is attributed to the fact that at this concentration, salt diffusion in the radial, and in particular the vertical direction take place in a smaller space and is affected to a greater extent by the wall effect. This is more pronounced in the middle portions of the cylinder (see concentrations 6, 10 and 14 cm from the bottom of the cylinder). So despite that rate 1 with the freezing temperature of -5°C was used, but the diameter was smaller than that required to allow free diffusion without submitting the salt ions to traffic jam (due to Fickian diffusion, wall effect and gravitational pull). A quick comparison of Fig. 9 with Fig. 5 emphasizes the aforementioned discussion as regards the effect of aspect ratio, in addition it is realized that container A permits more desalination to take place than container B (compare concentrations under similar occasions). This can be explained as follows: when we compare Figs. 5 and 9 at the same height, 17.5 cm from the bottom, the concentrations were 22.9 and 16.4 g/L in containers A and B in respective order. However, for container A there exists a height of 12.5 cm above that location, while for container B there was only 2.5 cm above this location. Moreover, when we compare the concentrations at identical distances from the top (2.5 cm), they were 10.9 and 16.4 g/L for containers A and B respectively, which may be attributed to the potential energy at different heights.

3.5. Effect of freezing of $\text{CuSO}_4 \cdot 5\text{H}_2\text{O}$ solution

In the present work the effect of the type of salts was investigated for the effect of its characteristics on the ability to remove it from aqueous solution by freezing. Accordingly, copper sulphate penta hydrate was selected for comparison with sodium chloride. This is shown in Fig. 10, in which four initial concentrations were studied using a cylinder A of dimensions $L = 30$ cm and $D = 8$ cm and the concentrations of which are shown in the legend of the figure. The latter illustrates the change in concentration from bottom to top for different initial $\text{CuSO}_4 \cdot 5\text{H}_2\text{O}$ concentrations. However, there is a difference in the change in the $\text{CuSO}_4 \cdot 5\text{H}_2\text{O}$ concentration by vertical distance, so that when C_i equals 5 g/L, the concentration at distance equals average 2.5 cm

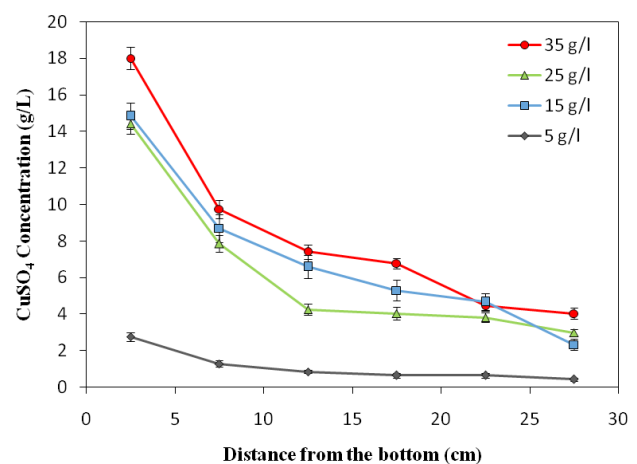


Fig. 10. The concentration profile of the frozen slices of containers B at freezing temperature of -5°C and different initial concentrations of $\text{CuSO}_4 \cdot 5\text{H}_2\text{O}$.

from the bottom is around 3 g/L while at the topmost (at 27.5 cm average distance) it becomes less than 1 g/L. At the same time, the maximum change from bottom to top took place when C_i is 35 g/L. However, in the medium concentrations the change in slope is less obvious than the higher concentration.

To compare this figure with Fig. 5 where sodium chloride of the same C was used, it is found that the curves are more smooth and the change in concentration from bottom to top is gradual and not subtle as that in case of $\text{CuSO}_4 \cdot 5\text{H}_2\text{O}$. This may be attributed to the nature of the salts where $\text{CuSO}_4 \cdot 5\text{H}_2\text{O}$ is much less soluble than NaCl, while NaCl is easily soluble in water and hard to form crystals during cooling; it is even known that NaCl can be produced commercially by evaporation rather than crystallization by cooling.

3.6. Effect of freezing of seawater

Fig. 11 presents the effect of distance from the periphery of the circular container to the center when seawater was used as solute. It is clear that at distance 7.5 cm from the periphery the concentration at all heights is identical as is shown by their lines or interceptions at this particular concentration. However, at 2.5 cm away from periphery the concentration changes with height, which may be attributed to diffusional reasons and settling velocity of individual particles, since gravitational acceleration is more pronounced near the periphery of the container owing to freezing, making the concentration more dilute, so that free settling takes place. On the other hand, at the center of the container it is observed that the difference in concentrations at the different heights studied is narrower than that near the periphery, and that at 17.5 cm which is the highest point from the bottom, the concentration was the lowest. In addition, at the other three heights (2.5, 7.5 and 12.5 cm) the concentrations are very close to each other. This may be attributed to the fact that at the center hindered settling takes place owing to the high concentration of salts which results in the concentrations being close to each other.

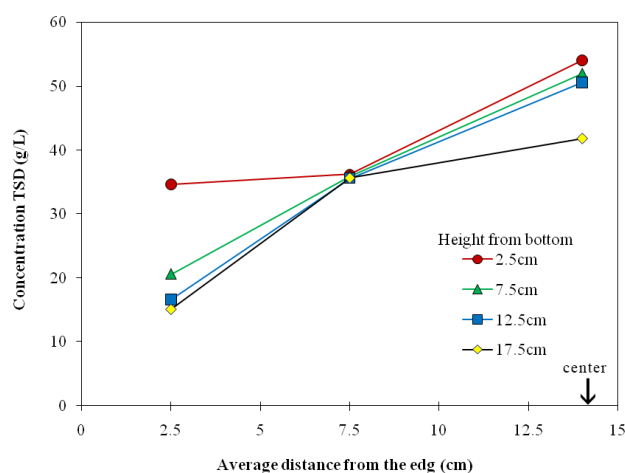


Fig. 11. The concentration distribution of seawater from the periphery of the circular container C to the center at freezing temperature of -5°C .

In Fig. 12, the same container C with the aspect ratio of 5/7 was used, however in this case the vertical distance from the bottom of the container was measured at four different distances (2.5, 7.5, 12.5, 17.5 cm) in this case the initial concentration used was 38.27 g/L (TDS). It is observed that the highest concentration was in the center section of the container followed by the next annular section at a concentration of about 35.84 g/L, which is almost identical with C_i . The outer annulus however produced much less concentrated solution indicating that as desalination takes place, the outermost portions of the water become frozen before the internal water. Therefore, ice is formed initially in those parts, which compels salts to be excluded from the salty water and pure ice crystals are formed. However, since the temperature is very low, salt diffusion is also very slow and therefore some salt remains in the ice cubes. And as ice formation proceeds the salt quantity increases which makes the concentration increase towards the center, therefore, maximum salts concentration is formed at the center.

Conclusively, for these reasons the outermost annulus is always the most desalinated fraction so that concentration increases radially and is maximum at the center. In addition, it is realized that the concentration increases downward in the cylindrical container C as shown by the curves in Fig. 12. This may be explained by considering that gravity and the settling velocity of individual particles have an effect on pulling down the ions to the bottom.

In Fig. 13, the effect of the distance from the edge to the center in container (D) is clarified. The latter is a pan of height 5 cm and diameter 33 cm. Starting with $C_i = 38.27$ g/L, it is observed that at the four distances selected there is a vast difference between the outermost annulus and the other three locations. This may be due to the cooling effect which takes place from the large circumference of the pan so that ice crystal formation is easier, also partly due to the very small height of the pan. Accordingly, the concentration dropped from 38.27 to about 15 g/L, which is less than half C_i . On the other hand, the concentration is 34 and 40.6 g/L at distances 6 and 16.5 cm (at the center) respectively, which indicates that desalination in the outermost annulus is much

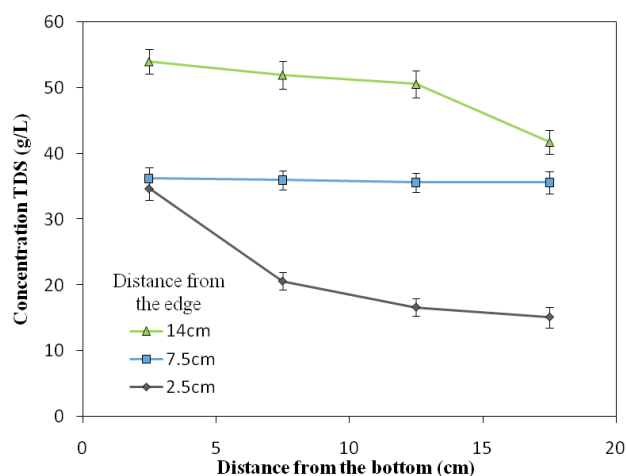


Fig. 12. The concentration profile of seawater of the circular container C at freezing temperature of -5°C .

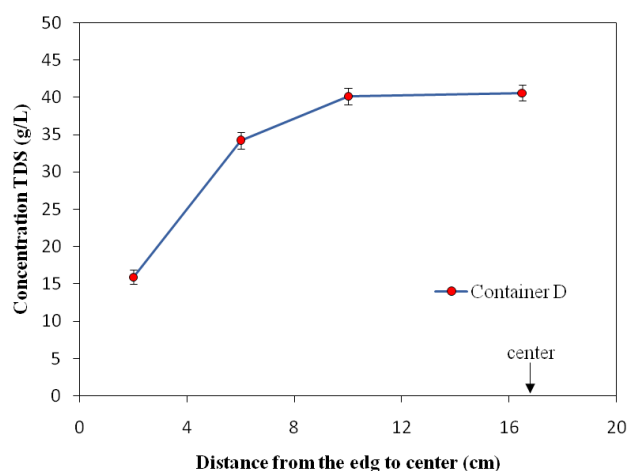


Fig. 13. The concentration distribution of seawater from the periphery of the circular container D to the center at freezing temperature of -5°C .

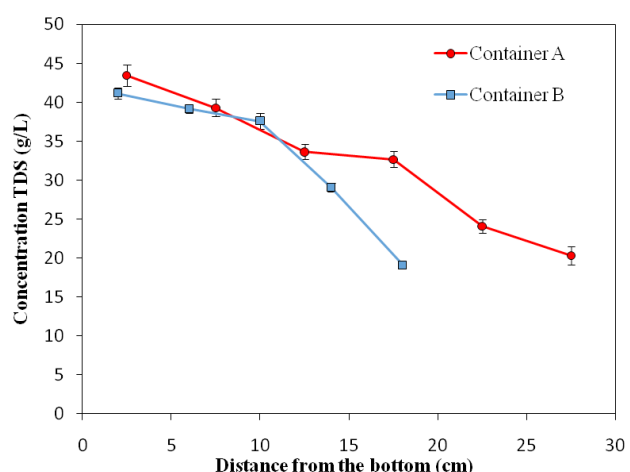


Fig. 14. The concentration profile of seawater of two containers A and B at freezing temperature of -5°C .

easier than the previous case in container C, in which the dimensions of the cylindrical container were 20 cm (height) and 28 cm (diameter) and aspect ratio = 5/8, since cooling leading to freezing takes place from top and bottom in the pan, as well as the side (periphery), which makes freezing take place very quickly getting rid of the salt to the center rapidly. At the same time, freezing also happens in the three other annuli, so that salt tends to diffuse simultaneously from the outermost annuli inwardly and from the cooled center outwardly, this makes a counter diffusion take place leading to a large zone of almost equal salt concentration.

Fig. 14 depicts the concentration change in the vertical direction of two containers of different aspect ratios, which were 3.75 and 3.33 for container A and B, respectively, as shown in the figure. The difference is sparse and the bottommost concentration is almost half the top section concentration. Despite that the initial concentration in both containers was 38.27 g/L, the final concentration at the topmost and at identical distances from the top (2.5 cm) were 20.3 and 19.1 g/L for container A and B respectively, which

are very close. Also, the final concentration at the bottom of both containers reached to almost equal concentrations (43.5 and 41.1 g/L, for A and B respectively). This may be attributed to the crystallization of salts comprising sea water which are different in sizes and shapes that interfere with the smooth settling of different crystal species. Moreover, it is worth noting that the container volumes vary from each other (container volume of A and B being 1508 and 565.5 cm^3 , respectively, which is equivalent to a volume ratio 2.67: 1) which is translated into more salt removal in case of A relative to B.

4. Conclusions

The freezing and solubility curves of NaCl–water system were calculated using PC-SAFT model with the corresponding melting temperatures and enthalpies of fusion of the pure substances using the binary parameter k_{ij} of -0.1793 for NaCl–water system. Desalination by freezing is characterized by the ability to reject salts as cooling takes place and ice is formed, producing saline water of lower salinity, depending on the initial concentration of the saline solution. It has been shown in the present work, that potable water can be produced from seawater (35 g/L) in three successive stages. Also concentration during freezing increases from top to bottom in the bottle and successively decreases toward the top. On the other hand, concentration increases radially from periphery to the center as was shown during freezing of saline water in a trough, from outer side, radially toward the center. It was also found that the direction of change in salinity in the vertical direction was greater than the radial direction, which means that gravity must have a contribution.

References

- [1] J.P. Chen, L.K. Wang, L. Yang, Y.-M. Zheng, Desalination of Seawater by Thermal Distillation and Electrodialysis Technologies, in: L.K. Wang, J.P. Chen, Y.-T. Hung, N.K. Shammam (Eds.) Membrane and Desalination Technologies, Humana Press, 2011, pp. 525–558.
- [2] T.-C. Chen, C.-D. Ho, Immediate assisted solar direct contact membrane distillation in saline water desalination, *J. Membr. Sci.*, 358 (2010) 122–130.
- [3] F. Banat, N. Jwaied, M. Rommel, J. Koschikowski, M. Wieghaus, Performance evaluation of the “large SMADES” autonomous desalination solar-driven membrane distillation plant in Aqaba, Jordan, *Desalination*, 217 (2007) 17–28.
- [4] D. Winter, J. Koschikowski, M. Wieghaus, Desalination using membrane distillation: experimental studies on full scale spiral wound modules, *J. Membr. Sci.*, 375 (2011) 104–112.
- [5] S.A. El-Agouz, Desalination based on humidification–dehumidification by air bubbles passing through brackish water, *Chem. Eng. J.*, 165 (2010) 413–419.
- [6] A. Eslamimanesh, M.S. Hatamipour, Mathematical modeling of a direct contact humidification–dehumidification desalination process, *Desalination*, 237 (2009) 296–304.
- [7] S.A. El-Agouz, A new process of desalination by air passing through seawater based on humidification–dehumidification process, *Energy*, 35 (2010) 5108–5114.
- [8] H. Li, Y. Gao, L. Pan, Y. Zhang, Y. Chen, Z. Sun, Electrosorptive desalination by carbon nanotubes and nanofibres electrodes and ion-exchange membranes, *Water Res.*, 42 (2008) 4923–4928.
- [9] B. Bornak, Desalination by Ion Exchange, in: Desalination, John Wiley & Sons, Inc., 2014, pp. 503–520.

- [10] A.M. Radhwan, Transient performance of a stepped solar still with built-in latent heat thermal energy storage, *Desalination*, 171 (2005) 61–76.
- [11] Z.S. Abdel-Rehim, A. Lasheen, Improving the performance of solar desalination systems, *Renewable Energy*, 30 (2005) 1955–1971.
- [12] M.M. Naim, M.A. Abd El Kawi, Non-conventional solar stills Part 2. Non-conventional solar stills with energy storage element, *Desalination*, 153 (2003) 71–80.
- [13] M. Naim, M. Elewa, A. El-Shafei, A. Moneer, Desalination of simulated seawater by purge-air pervaporation using an innovative fabricated membrane, *Water Sci. Technol.*, 72 (2015) 785–793.
- [14] Z.L. Xie, M. Hoang, D. Ng, C. Doherty, A. Hill, S. Gray, Effect of heat treatment on pervaporation separation of aqueous salt solution using hybrid PVA/MA/TEOS membrane, *Sep. Purif. Technol.*, 127 (2014) 10–17.
- [15] B. Liang, K. Pan, L. Li, E.P. Giannelis, B. Cao, High performance hydrophilic pervaporation composite membranes for water desalination, *Desalination*, 347 (2014) 199–206.
- [16] M.M. Elewa, A.A. El-Shafei, A.A. Moneer, M.M. Naim, Effect of cell hydrodynamics in desalination of saline water by sweeping air pervaporation technique using innovated membrane, *Desal. Water Treat.*, 57 (2016) 23293–23307.
- [17] M.M. Naim, A.A. El-Shafei, A.A. Moneer, M.M. Elewa, W.G. Kandeel, Bulk liquid pertraction of NaCl from aqueous solution using carrier-mediated transport, *Environ. Technol.*, 37 (2016) 495–504.
- [18] M.M. Naim, A.A. Monir, Desalination using supported liquid membranes, *Desalination*, 153 (2003) 361–369.
- [19] A.A. El-Shafei, A.A. Moneer, M.M. Elewa, M.M. Naim, Kinetics of transport of sodium chloride using supported liquid pertraction, *Desal. Water Treat.*, 57 (2016) 23280–23292.
- [20] T.J. Welgemoed, C.F. Schutte, Capacitive deionization technology™: An alternative desalination solution, *Desalination*, 183 (2005) 327–340.
- [21] M.-W. Ryoo, G. Seo, Improvement in capacitive deionization function of activated carbon cloth by titania modification, *Water Res.*, 37 (2003) 1527–1534.
- [22] L. Zou, G. Morris, D. Qi, Using activated carbon electrode in electrosorptive deionisation of brackish water, *Desalination*, 225 (2008) 329–340.
- [23] Z. Spitalisky, D. Tasis, K. Papagelis, C. Galiotis, Carbon nanotube-polymer composites: chemistry, processing, mechanical and electrical properties, *Progr. Polym. Sci.*, 35 (2010) 357–401.
- [24] Y. Oren, Capacitive deionization (CDI) for desalination and water treatment- past, present and future (a review), *Desalination*, 228 (2008) 10–29.
- [25] Y. Mandri, A. Rich, D. Mangin, S. Abderafi, C. Bebon, N. Semlali, J.-P. Klein, T. Bounahmidi, A. Bouhaouss, Parametric study of the sweating step in the seawater desalination process by indirect freezing, *Desalination*, 269 (2011) 142–147.
- [26] J. Ulrich, H. Glade, Melt Crystallization – Fundamentals, Equipment and Applications, in: S. Verlag (Ed.), Aachen, 2003, pp. 7–40.
- [27] B. Habib, M. Farid, Heat transfer and operating conditions for freeze concentration in a liquid–solid fluidized bed heat exchanger, *Chem. Eng. Process.*, 45 (2006) 698–710.
- [28] Y. Cerri, A new ideal evaporative heating cycle, *Int. J. Heat Mass Transfer*, 46 (2003) 2967–2974.
- [29] M.V. Rane, Y.S. Padiya, Heat pump operated freeze concentration system with tubular heat exchanger for seawater desalination, *Energy Sustain. Develop.*, 15 (2011) 184–191.
- [30] J. Chang, J. Zuo, K.-J. Lu, T.-S. Chung, Freeze desalination of seawater using LNG cold energy, *Water Res.*, 102 (2016) 282–293.
- [31] P. Wang, T.-S. Chung, A conceptual demonstration of freeze desalination–membrane distillation (FD–MD) hybrid desalination process utilizing liquefied natural gas (LNG) cold energy, *Water Res.*, 46 (2012) 4037–4052.
- [32] W.E. Johnson, Indirect freezing, *Desalination*, 31 (1979) 417–425.
- [33] J. Ulrich, H. Glade, *Melt Crystallization: fundamentals, equipment and applications*, Shaker Verlag, Aachen, 2003.
- [34] F.G.F. Qin, J.C. Zhao, A.B. Russell, X.D. Chen, J.J. Chen, L. Robertson, Simulation and experiment of the unsteady heat transport in the onset time of nucleation and crystallization of ice from the subcooled solution, *Int. J. Heat Mass Transfer*, 46 (2003) 3221–3231.
- [35] K.J. Kim, S.H. Lee, J. Ulrich, Experimental thermal conductivity of ice crystalline layer in layer melt crystallization, *J. Indust. Eng. Chem.*, 9 (2003) 111–116.
- [36] R. Guardani, S.M.S. Neiro, H. Büllau, J. Ulrich, Experimental comparison and simulation of static and dynamic solid layer melt crystallization, *Chem. Eng. Sci.*, 56 (2001) 2371–2379.
- [37] Y. Shirai, M. Wakisaka, O. Miyawaki, S. Sakashita, Effect of seed ice on formation of tube ice with high purity for a freeze wastewater treatment system with a bubble-flow circulator, *Water Res.*, 33 (1999) 1325–1329.
- [38] M.M. Mohamed, Solidification of phase change material on vertical cylindrical surface in holdup air bubbles, *Int. J. Refrigeration*, 28 (2005) 403–411.
- [39] U. Shafique, J. Anwar, M.A. Munawar, W.-u. Zaman, R. Rehman, A. Dar, M. Salman, M. Saleem, N. Shahid, M. Akram, A. Naseer, N. Jamil, Chemistry of ice: migration of ions and gases by directional freezing of water, *Arab. J. Chem.*, 4 (2011) 51–54.
- [40] A.A. Madani, S.E. Aly, A combined RO/freezing system to reduce inland rejected brine, *Desalination*, 75 (1989) 241–258.
- [41] F. Dolezalek, Zur Theorie der binären Gemische und konzentrierten Lösungen, *Z. phys. Chem.*, 64 (1908) 727–747.
- [42] F. Tumakaka, I.V. Prikhodko, G. Sadowski, Modeling of solid–liquid equilibria for systems with solid–complex phase formation, *Fluid Phase Equilib.*, 260 (2007) 98–104.
- [43] Y.-H. Fu, S.I. Sandler, H. Orbey, A Modified UNIQUAC Model that includes Hydrogen bonding, *Indust. Eng. Chem. Res.*, 34 (1995) 4351–4363.
- [44] J. Gross, G. Sadowski, Perturbed-Chain SAFT: An equation of state based on a perturbation theory for chain molecules, *Indust. Eng. Chem. Res.*, 40 (2001) 1244–1260.
- [45] J. Gross, J. Vrabec, An equation-of-state contribution for polar components: dipolar molecules, *AIChE J.*, 52 (2006) 1194–1204.
- [46] J. Gross, G. Sadowski, Application of the perturbed-chain SAFT equation of state to associating systems, *Indust. Eng. Chem. Res.*, 41 (2002) 5510–5515.
- [47] J. Gross, G. Sadowski, Modeling polymer systems using the perturbed-chain statistical associating fluid theory equation of state, *Indust. Eng. Chem. Res.*, 41 (2002) 1084–1093.
- [48] J. Gross, O. Spuhl, F. Tumakaka, G. Sadowski, Modeling copolymer systems using the perturbed-chain SAFT equation of state, *Indust. Eng. Chem. Res.*, 42 (2003) 1266–1274.
- [49] F. Ruether, G. Sadowski, Solubility of Complex Natural and Pharmaceutical Substances, in: H.-J. Bart, S. Pilz (Eds.) *Industrial Scale Natural Products Extraction*, Wiley-VCH Verlag & Co. KGaA, Weinheim, Germany, 2011, pp. 27–54.
- [50] W.G. Chapman, G. Jackson, K.E. Gubbins, Phase equilibria of associating fluids, *Mol. Phys.*, 65 (1988) 1057–1079.
- [51] M.S. Wertheim, Fluids with highly directional attractive forces. II. Thermodynamic perturbation theory and integral equations, *J. Stat. Phys.*, 35 (1984) 35–47.
- [52] M.S. Wertheim, Fluids with highly directional attractive forces. I. Statistical thermodynamics, *J. Stat. Phys.*, 35 (1984) 19–34.
- [53] M.S. Wertheim, Fluids of dimerizing hard spheres, and fluid mixtures of hard spheres and dispheres, *J. Chem. Phys.*, 85 (1986) 2929–2936.
- [54] J.A. Barker, D. Henderson, Perturbation theory and equation of state for fluids: the Square-Well Potential, *J. Chem. Phys.*, 47 (1967) 2856–2861.
- [55] J.A. Barker, D. Henderson, Perturbation theory and equation of state for fluids. II. A successful theory of liquids, *J. Chem. Phys.*, 47 (1967) 4714–4721.
- [56] M. Kleiner, G. Sadowski, Modeling of polar systems using PCP-SAFT: an approach to account for induced-association interactions, *J. Chem. Phys. C.*, 111 (2007) 15544–15553.

- [57] W.G. Chapman, K.E. Gubbins, G. Jackson, M. Radosz, New reference equation of state for associating liquids, *Indust. Eng. Chem. Res.*, 29 (1990) 1709–1721.
- [58] J.P. Wolbach, S.I. Sandler, Using molecular orbital calculations to describe the phase behavior of cross-associating mixtures, *Indust. Eng. Chem. Res.*, 37 (1998) 2917–2928.
- [59] J.M. Prausnitz, R.N. Lichtenthaler, E.G. Azevedo, *Molecular Thermodynamics of Fluid-Phase Equilibria*, Prentice Hall, 1969.
- [60] F.G.F. Qin, X.D. Chen, K. Free, Freezing on subcooled surfaces, phenomena, modeling and applications, *Int. J. Heat Mass Transfer*, 52 (2009) 1245–1253.
- [61] G.L. Stepakoff, D. Siegelman, R. Johnson, W. Gibson, Development of a eutectic freezing process for brine disposal, *Desalination*, 15 (1974) 25–38.
- [62] K.S. Pitzer, J.C. Peiper, R.H. Busey, Thermodynamic properties of aqueous sodium chloride solutions, *J. Phys. Chem. Ref. Data*, 13 (1984) 1–102.
- [63] P.K. Rohatgi, *Dendritic Solidification of Aqueous Solutions*, in: Massachusetts Institute of Technology (MIT), 1964.
- [64] R. Masoudi, B. Tohidi, R. Anderson, R.W. Burgass, J. Yang, Experimental measurement and thermodynamic modelling of clathrate hydrate equilibria and salt solubility in aqueous ethylene glycol and electrolyte solutions, *Fluid Phase Equilib.*, 219 (2004) 157–163.
- [65] W. van der Tempel, Eutectic freeze crystallization: separation of salt and ice, in: process and energy, Faculty of Mechanical, Maritime and Material Engineering, TU Delft, Delft University of Technology, 2012, pp. 58.